Contributor's note:

Imaging Nanoscale Inhomogeneities in As-Grown MoS$_2$ by Tip-Enhanced Photoluminescence in Gap-less Mode

Alvaro Rodriguez, Tim Verhagen, Martin Kalbac, Jana Vejpravova, Otakar Frank*

Dr. A. Rodriguez, Dr. M. Kalbac, Dr. O. Frank
J. Heyrovský Institute of Physical Chemistry, Academy of Sciences of the Czech Republic, Dolejškova 2155/3, 182 23 Prague, Czech Republic
E-mail: otakar.frank@jh-inst.cas.cz

Dr. T. Verhagen, Dr. J. Vejpravova
Department of Condensed Matter Physics, Faculty of Mathematics and Physics, Charles University, Ke Karlovu 5, 121 16, Prague 2, Czech Republic

Abstract

Methods for nanoscale material characterization are in an ever-increasing demand, especially those, which can provide a broader range of information at once. Near-field techniques based on combinations of scanning probe microscopy (SPM) and Raman or photoluminescence spectroscopy (TERS or TEPL) belong, thanks to their capabilities and fast development, to strong candidates for becoming widespread across the scientific community as did the SPM and Raman microscopy only a decade or two ago. However, in particular for monolayer, 2D materials, the utilization of the tip-enhanced methods has relied so far mostly on the 'gapped' mode, which necessitates the material to be transferred onto a metallic substrate, incurring damaging changes in the process. The present work shows that even the gap-less TEPL performed directly on as-grown MoS$_2$ monolayer samples without any pretreatment is also capable of providing nanoscale hyperspectral imaging. The mapping resolution down to few tens of nanometers clearly distinguishes homogeneous layer interiors from defective edge fronts in the grown monolayers, in contrast to mechanically exfoliated flakes, which show topography- and contamination-related heterogeneities in the whole flake area. The TEPL

interpretation is aided by local surface potential and capacitance measurements, performed with the same AFM tip.

Standard optical techniques such as Raman or photoluminescence (PL) microspectroscopies give plentiful information about both structural and optoelectronic properties of layered transition metal dichalcogenides (TMDs). [1] However, the spatial resolution of these techniques is diffraction limited where the Abbe diffraction limit of the resolution, d, is equal to $d = \lambda/2$ NA with λ the wavelength of the irradiated light and NA the numerical aperture of the objective. For a typical Raman or PL experiment, with visible light and an objective with a NA around 1 results in a diffraction limited resolution of several hundreds of nanometers which hinders the understanding of the material's properties at the nanoscale. One possibility to overcome this issue is using an apex of an atomic force microscope (AFM) or scanning tunneling microscope (STM) tip (nanoantenna) to improve the intensity of the optical signal in the near-field due to the combination of a lightning rod effect and a surface plasmon resonance at the metallized tip. [2] In general, tip-enhanced techniques improved greatly during the last years, reaching a resolution around tens of nanometers and enhancement factors of 10^7-10^{10} in the near-field [3] Even so, most works deal with single spectrum acquisition and only the past few years saw studies concerning tip-enhanced imaging methods, e.g. refs [4–7].

TMDs usually exhibit a strong PL associated to an exciton transition. In particular, MoS_2 monolayer presents two direct optical transitions of the A and B excitons at approximately 1.8 eV and 2 eV respectively which PL energy can easily be shifted towards higher or lower energies depending on environment conditions.[8] For instance, the PL of chemical vapor deposited (CVD) MoS_2 monolayers have been found to shift towards lower energies after transferring to a different substrate with a polymer due to defects generated during the transfer.[9] Moreover, one can find a great variety of results in the literature when comparing quantitative values of PL due to the diverse synthesis or exfoliation methods used.[10,11]

Nanoscale heterogeneities such as defects and wrinkles are most likely responsible of this issue, as shown for graphene previously.[12] In this sense, the at least 10 to 20 times improved spatial resolution of tip-enhanced methods can help us to understand how nanoscale heterogeneities may affect the optoelectronics properties of these materials and eventually improve the synthesis methods to obtain optimal CVD flakes for a specific application. Some works on Raman nanoscale characterization of TMDs materials have been reported so far, most of them obtained in the so-called 'gap mode' when the layers were first transferred on gold substrates to localize and intensify the near-field between the tip and the substrate.[13] However, while both the enhancement and spatial resolution are improved, the transfer inevitably leads to damage in the interrogated material. The obtained information on the quality and properties of the grown layers has thus only a limited value. Moreover, PL is quenched when MoS_2 is supported on a freshly prepared gold[14] avoiding the possibility of measuring tip-enhanced photoluminescence (TEPL) under this favorable conditions.

Here, we report a study of different CVD grown MoS_2 flakes by TEPL in the 'gap-less' regime, i.e. where the near-field is produced solely by the tip. We have measured TEPL of as-grown MoS_2 on SiO_2/Si substrates with no transfer or other treatment. Different CVD flakes were examined in order to verify heterogeneities of the flakes, such as variations of PL at nanoscale due to defects. The results are compared to data obtained on mechanically exfoliated MoS_2, with a special attention paid to the edges of the flakes.

Figure 1a shows the topography image of a MoS_2 flake grown by CVD. Thickness of the flake is approximately 0.7 nm, which is consistent with the thickness reported for a monolayer.[15] The height profile (Figure 1c) reveals that edges are 2 nm taller than the interior of the flake. Figure 1b shows the contact potential difference (CPD) image measured by Kelvin Probe Force Microscopy (Frequency Modulated, KPFM-FM). The CPD image shows a homogeneous potential in the interior of the flake and only at the edges one can observe different values,

correlating fairly well with the topography image. The CPD inside the flake is approx. 400-500 mV lower compared to the substrate. The edge shows CPD values lowered by an additional 100 mV compared to the flake interior (Figure 1d). No noticeable variation in CPD is detected inside the flake probably due to a lower resolution of the KPFM compared to the topography. Finally, micro Raman and PL spectra (far-field) collected at the center of the flake are shown in Figure 1(e-f).
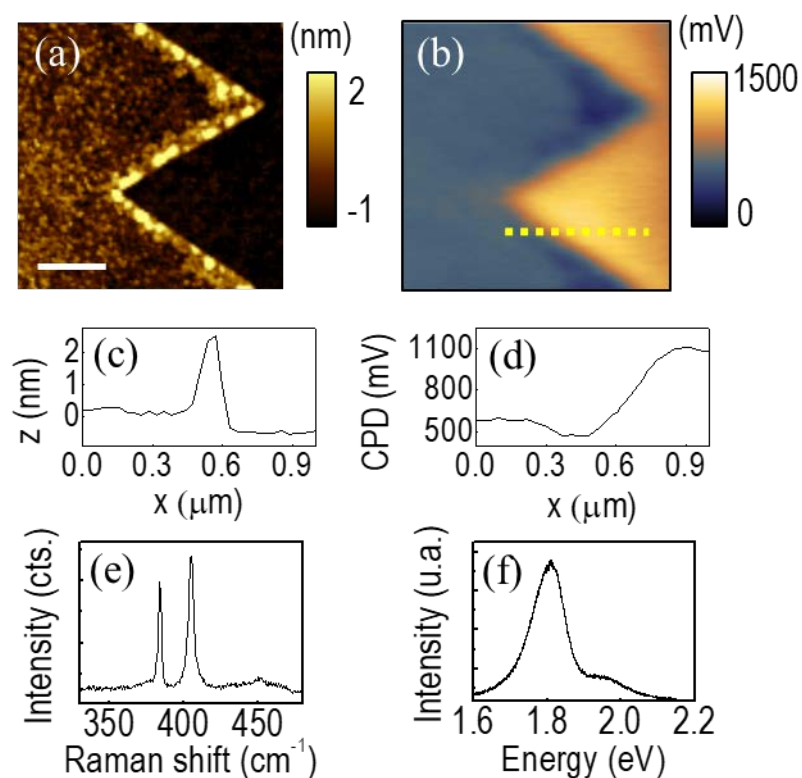

Figure 1. CVD grown MoS_2 monolayer: (a) topography and (b) CPD images. (c) Height profile across the edge, and (d) CPD profile across the edge, (e) Raman spectrum, (f) photoluminescence (PL). Scale bar is 500 nm.

Raman spectrum present the E_{2g} and A_{1g} modes separated by less than 21 cm^{-1}, a value typical for CVD-grown monolayer MoS_2 [6]. In the PL spectrum, A and B excitons appear at 1.81 eV

and 1.96 eV respectively. These features are typical for CVD MoS_2 monolayer, which confirm the monolayer thickness.

At this point, it would be beneficial to gain information of the PL with a similar resolution as the AFM images. As commented above, micro PL resolution is limited to hundreds of nanometers and one approach to overcome the diffraction limit is to perform TEPL measurements.

TEPL measurements were obtained by side illumination of a silver coated AFM tip with a red laser excitation (633 nm). Far and near-field images were collected by switching the AFM from tapping to contact mode, respectively, while scanning the sample in tapping mode and measuring the PL spectrum at each point when the tip is close to the sample (near-field spectrum) and far from the sample (far-field spectrum). Side illumination results to a rather strong far field and non-circular laser spot at the sample.[16] To obtain the sole near-field contribution, it is necessary to subtract the far-field contribution to obtain the actual near-field spectrum for each map point. In all the cases, both far and subtracted near-field PL spectra were fitted to a single asymmetric pseudo-Voight function to account for the superposition of both the neutral (A^0) and charged exciton (A^-, trion), which are difficult to deconvolute during high-speed TEPL mapping. **Figure 2a** shows the near-field (blue line), far-field (black line) and corrected near–field PL spectra (red line) collected in the interior area of the flake. The spectra in the Figure 2b, correspond to the edges of the flake where the PL enhancement is higher. Figure 2c-d shows maps of the intensity and the energy, respectively, of the A^0 exciton in the near-field conditions, after subtracting the far-field contribution. PL intensity and energy values vary only slightly in the interior of the flake and only the edges, approx. 80 nm wide, show a significant change in the PL. The recognition of the features at the edges are possible only thanks to the dramatic improvement of the lateral resolution compared to the far-field measurements (Supporting Information, Figure S1).
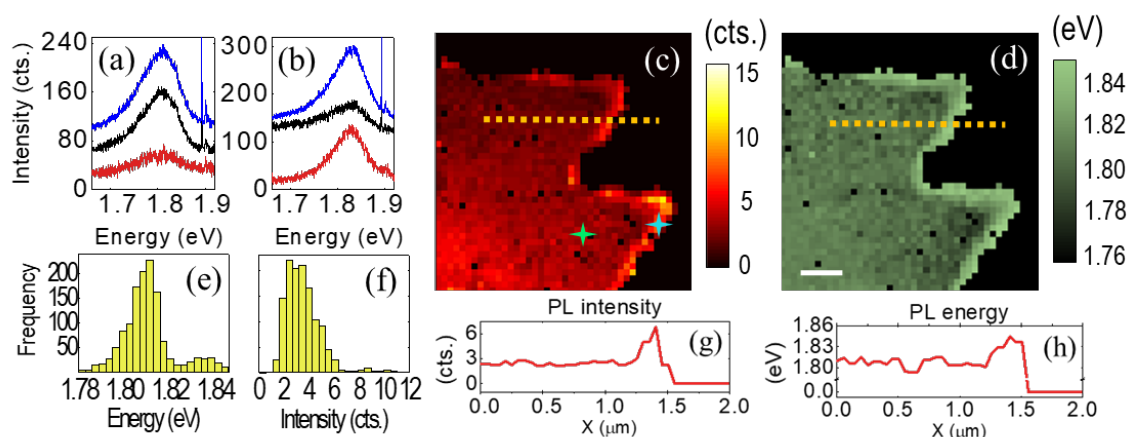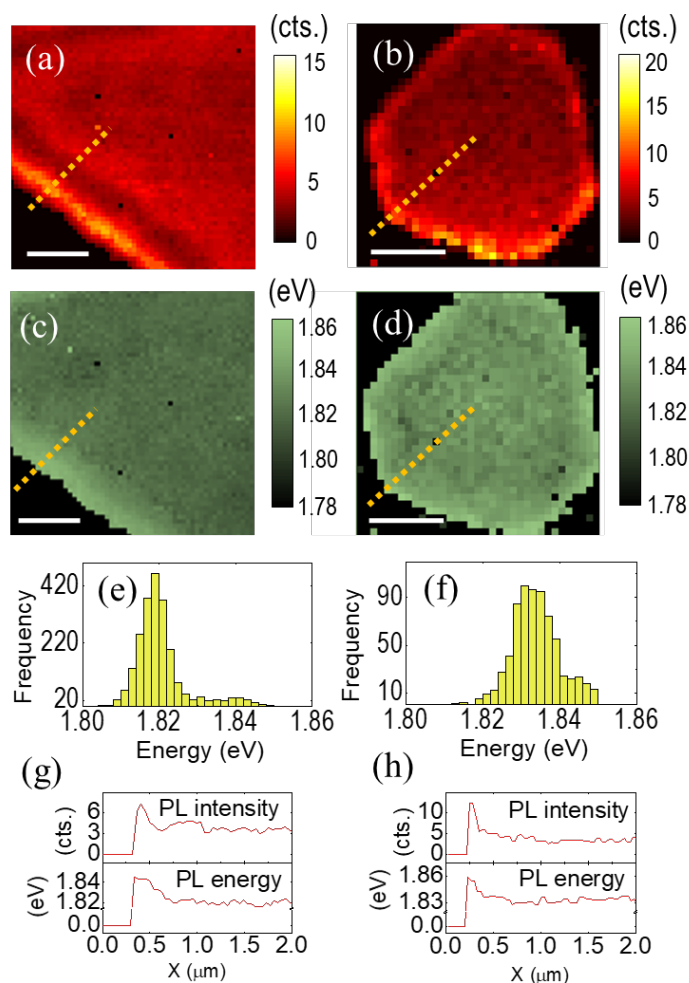
Figure 2. TEPL of CVD MoS$_2$ monolayers: PL spectra in the near-field (blue line), far-field (black line) and subtracted (red line) collected at (a) the interior area of the flake and (b) the edge of the flake. The sharp peaks in the spectra are Raman bands of silicon and MoS$_2$ (from left to right) (c) Near-field PL intensity and (d) energy maps. Green and blue marks indicate the areas where spectra in (a) and (b) were collected, respectively. Histograms of (e) near-field PL intensity and (f) PL energy from the whole map. (g) PL intensity and (h) PL energy profiles across the flake edge in the near-field map Scale bar is 500 nm.

Figure 2 reveals two clear conclusions: (i) Even in the gap-less mode, TEPL on single layer MoS$_2$ on a dielectric substrate can provide high enough enhancement to conduct hyper-spectral mapping with lateral resolution down to tens of nanometers allowing to resolve very detailed features compared to the far-field imaging. (ii) The resolved PL is clearly more intense at the edges of the flake and blue-shifted compared to the flake interior. We have extracted both the intensity and energy profiles from the near-field image across the flake edge (Figure 2g-h). The profiles clearly show the correlated abrupt increase of PL intensity and energy approaching the edge. The intensity increase at the edge is almost two-fold, the energy blue-shifted by approximately 25 meV. This can also be observed in the histograms presented in Figure 2e-f. There are two distinct maxima in the PL energy distribution, one centered at 1.81 eV for the flake interior and the second one at 1.84 eV for the edges (Figure 2e). The PL blue-shift and intensity increase is strongly reminiscent of the effect of the decreasing population of charged excitons, the trions, by electric field,[17] molecular doping,[18] or defects.[10] As the excessive

charges are neutralized, the lower energy trion PL peak becomes weaker and, in the same time, the higher energy neutral exciton PL peak becomes significantly stronger. The same effect can be facilitated by defects. For example, Tongay et al.[10] reported a three times increase of the PL integrated intensity as well as a blue-shift of the PL maxima by 20 meV caused by α particles irradiation in the presence of electron-withdrawing N_2 molecules which are bound to the formed defect sites. The generated defect density was estimated to 6×10^{11} cm-2.[10] A similar effect can be observed because of the most likely incomplete growth on the edge.[7] The surface potential change further corroborates the influence of charge/defects on the populations of excitons and the observed changes in PL.

It is well known that MoS_2 growth by CVD is very sensitive to the synthesis conditions, and flakes with different shape can be obtained by varying the reaction conditions.[19,20] Depending on the local sulfur concentration along the sample, MoS_2 flakes with different shapes were selected and TEPL was measured to verify the universality of the edge-related changes. PL near field maps of both a triangular and hexagonal MoS_2 flakes are presented in **Figure 3a-b** (PL intensity) and 3c-d (PL energy). Detailed topography analysis can be found in Figure S2. In these cases, "interior" PL is centered at approximately 1.82 and 1.83 eV for the triangular a hexagonal flake, respectively (Figure e-f). Apparently, besides the slight shift of the PL distribution, the results are very similar to the previous case and once again, the edges exhibit more intense and blue shifted PL compared to the central part of the flake, as can be observed in the intensity and energy profiles (Figure 3g-h).

Figure 3. TEPL of CVD MoS$_2$ monolayers with different shape: Near-field PL intensity maps for (a) triangular and (b) hexagonal. Near-field PL energy maps for (c) triangular and (d) hexagonal flake. Histograms of the PL energy distribution for triangular (e) and (f) hexagonal flake. PL intensity and energy profiles across the flake edges (indicated by dashed yellow lines in the maps for (g) triangular and (h) hexagonal flake. Scale bar is 500 nm.

We can assume that despite the local variation in sulfur concentration resulting into the growth of flakes with different shapes, edges and growth kinetics, the defect occurrence at the edges connected with electron depletion is universal in our type of growth. The evidenced PL intensity increase at the edges is, actually, inverse to a previous study, conducted with TEPL on as-grown MoS$_2$ from MoO$_3$ precursor.[6] The reasons for the difference can be looked for in the growth process, however, many parameters varied between our and the mentioned work (precursor: MoO$_2$ vs. MoO$_3$, growth temperature: 850 °C vs. 700 °C, carrier gas: Ar vs N$_2$, in the presented

work and in ref. [6], respectively). It is clear that further detailed investigations are necessary to uncover the details of the growth process and relate them to the structural and excitonic properties of the material.

We have successfully applied gap-less TEPL to characterize as-grown CVD MoS_2 flakes. To put our observations in contrast, we focus now on a mechanically exfoliated flake. Topography image is shown in **Figure 4a** and it shows a flake formed by different number of layers (increasing from the edge). Additional AFM images are shown in Figure S3 (Supporting information). A big wrinkle (100 nm wide, 15 nm high), through the whole length in the middle of the image, and two smaller ones, approximately perpendicular to the edge, can be observed in the monolayer region. These features and the separation between layers are better observed in both CPD and capacitance images (Figure S3).
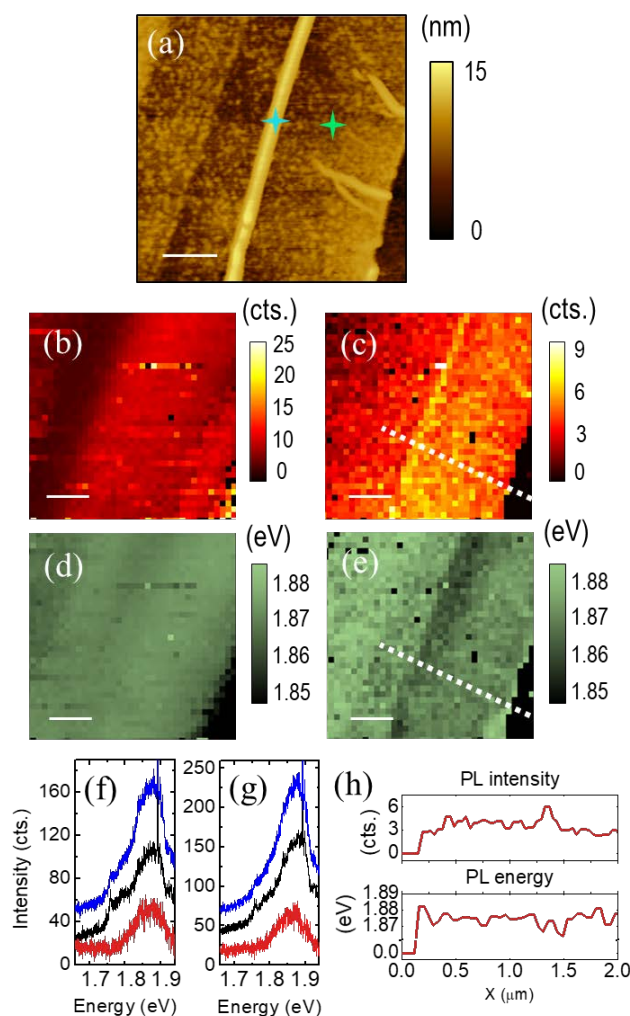
Figure 4. TEPL of exfoliated MoS$_2$ flake. (a) AFM topography image. Green and blue marks indicate the areas where spectra in (f) and (g) were collected, respectively (b) Far- and (c) near-field PL intensity maps and (d) far- and (e) near-field PL energy maps. PL spectra in the near-field (blue line), far-field (black line) and subtracted (red line) collected at (f) the 'flat' area of the flake and (g) the big wrinkle. (h) PL intensity and energy profiles along near-field maps. Scale bar is 500 nm.

In Figure 4b-e the far- and near-field PL intensity and PL energy maps of the exfoliated flake are shown for comparison. Both the big and small wrinkles are distinguished in the near-field maps. Selected spectra are shown in Figure 4f-g. The spectra obtained from the big wrinkle (Figure 4g, blue marked in Figure 4a) show a slightly higher enhancement than the flat monolayer region (Figure 4f, green marked in Figure 4a). From the maps we can conclude that

the three wrinkles exhibit higher PL intensity than the rest of the flake as well as shifts in the energy. Curiously, the big wrinkle red-shifts the PL energy, which is counterintuitive, since small compressive strain should cause band-gap opening, i.e. PL energy increase. [21] On the other hand, in a similar case, albeit with few layer MoS_2 and much wider wrinkles, the unexpected red-shift was explained by the effects of energy funneling. [22] In contrast, the PL energy at the small wrinkles is blue-shifted, i.e., probably the compressive effects dominate in that case. However, the most important observation with respect to the CVD samples, is the rather uniform PL in terms of both intensity and energy going from the interior of the flake towards the edge. No tonality can be observed in the CPD and capacitance images either (Figure S3), confirming the defect front at the edges in the CVD samples is inherent to the growth process, and not to, e.g., ageing of the sample in laboratory conditions.

In conclusion, we have shown that gap-less Tip-Enhanced Photoluminescence on monolayer MoS_2 is capable of providing signals intense enough to thoroughly investigate as-grown samples on a dielectric substrate with a lateral resolution down to tens of nanometers. Consequently, there is no need to transfer the samples to a metallic (gold, silver) substrate before such an analysis takes place, thereby avoiding modification (or even damage) and contamination of the sample by the transfer process. Fitting the spectra in every map point reveals that monolayer MoS_2 flakes exhibit heterogeneities in samples grown by chemical vapor deposition and prepared by mechanical exfoliation. The edges of the CVD flakes feature, in all the samples, an increased intensity and a blue shift of the PL band. The PL results correlate well with surface potential measurements, which manifest different values between the edges and the flake interior. The changes in the PL signatures as well as in the surface potential can be explained by the presence of growth-induced defects and related charge compensation through moieties, which readily sorb onto the defect sites. On the other hand, the interior of the CVD flakes is rather homogeneous in the single layer limit. Both these observations are in a stark

contrast with measurements of exfoliated layers. In this case, the edges have similar PL intensity and energy compared to the flake interior. The variations in PL signature are clearly visible in the whole flake, caused by topographical corrugations like wrinkles or bubbles and contamination.

Experimental Section

Sample preparation

The MoS_2 monolayers were grown using chemical vapor deposition (CVD) using MoO_2 (Sigma Aldrich #234761) and S (Sigma Aldrich #344621) as sources by atmospheric pressure CVD. [5,20] A 3 x 1 cm² piece of Si/SiO₂ (300 nm) substrate was cleaned with acetone and isopropanol and subsequently placed phase down on a quartz crucible containing 30 mg MoO_2 powder. The crucible was installed in the middle of the oven and 90 mg S was placed just outside the oven. The tube was flushed with Ar gas at room temperature, hereafter the MoS_2 growth was initiated with an Ar flow of 120 sccm. The temperature was gradually increased to the growth temperature of 1123 K at 40 K/min, and held there for 10 minutes. After the growth, the oven was opened and the sample was quickly cooled to room temperature in the Ar flow of 120 sccm. MoS_2 exfoliated layer was prepared from MoS_2 bulk (GQ graphene) by mechanical exfoliation onto PDMS and transferred with a customized transfer station on top of a SiO₂/Si substrate previously cleaned with acetone and isopropanol.

AFM and Raman details

Topography, CPD and capacitance images were collected with AIST-NT SPM in KPFM-FM mode. ACCESS-EFM probes (tip-view), App Nano, k = 2.7 N.m⁻¹, f = 60 kHz covered by Pt-Ir.

Micro Raman and PL spectra were collected with LabRAM Evolution spectrometer using 532 nm laser excitation with 1800 and 300 l/mm gratings, respectively.

TEPL measurements were performed with LabRAM HR Evolution spectrometer coupled to AIST-NT SPM with 633 nm laser excitation, 300 l/mm grating and using side optical access. ACCESS-FM probes (App Nano, tip/view, k = 2.7 N.m^{-1}, f = 60 kHz) were covered by approx. 70 nm of silver by magnetron sputtering.

Supporting Information
Supporting Information is available from the Wiley Online Library or from the author.

Received: ((will be filled in by the editorial staff))
Revised: ((will be filled in by the editorial staff))
Published online: ((will be filled in by the editorial staff))

References

[1]   H. Li, Q. Zhang, C. C. R. Yap, B. K. Tay, T. H. T. Edwin, A. Olivier, D. Baillargeat, *Adv. Funct. Mater.* **2012**, *22*, 1385.

[2]   a) R. M. Stöckle, Y. D. Suh, V. Deckert, R. Zenobi, *Chem. Phys. Lett.* **2000**, *318*, 131; b) L. Meng, T. Huang, X. Wang, S. Chen, Z. Yang, B. Ren, *Opt. Express* **2015**, *23*, 13804; c) R. Beams, L. G. Cançado, A. Jorio, A. N. Vamivakas, L. Novotny,

14

Nanotechnology **2015**, *26*, 175702.

[3]   a) B. Pettinger, P. Schambach, C. J. Villagómez, N. Scott, *Annu. Rev. Phys. Chem.*
2012, *63*, 379; b) R. Zhang, Y. Zhang, Z. C. Dong, S. Jiang, C. Zhang, L. G. Chen, L.
Zhang, Y. Liao, J. Aizpurua, Y. Luo, J. L. Yang, J. G. Hou, *Nature* **2013**, *498*, 82.

[4]   a) T. Yano, T. Ichimura, S. Kuwahara, F. H'Dhili, K. Uetsuki, Y. Okuno, P. Verma, S.
Kawata, *Nat. Commun.* **2013**, *4*, 2592, b) W. Su, N. Kumar, S. Mignuzzi, J. Crain, D.
Roy, *Nanoscale* **2016**, *8*, 10564; c) N. J. Borys, E. S. Barnard, S. Gao, K. Yao, W. Bao,
A. Buyanin, Y. Zhang, S. Tongay, C. Ko, J. Suh, A. Weber-Bargioni, J. Wu, L. Yang,
P. J. Schuck, *ACS Nano* **2017**, *11*, 2115; d) Y. Okuno, O. Lancry, A. Tempez, C.
Cairone, M. Bosi, F. Fabbri, M. Chaigneau, *Nanoscale* **2018**, *10*, 14055; e) K. K. H.
Smithe, A. V Krayev, C. S. Bailey, H. R. Lee, E. Yalon, Ö. B. Aslan, M. Muñoz Rojo,
S. Krylyuk, P. Taheri, A. V Davydov, T. F. Heinz, E. Pop, *ACS Appl. Nano Mater.*
2018, *1*, 572; f) W. Su, N. Kumar, A. Krayev, M. Chaigneau, *Nat. Commun.* **2018**, *9*,
2891; g) N. S. Mueller, S. Juergensen, K. Höflich, S. Reich, P. Kusch, *J. Phys. Chem.*
C **2018**, *122*, 28273.

[5]   I. Bilgin, F. Liu, A. Vargas, A. Winchester, M. K. L. Man, M. Upmanyu, K. M. Dani,
G. Gupta, S. Talapatra, A. D. Mohite, S. Kar, *ACS Nano* **2015**, *9*, 8822.

[6]   W. Bao, N. J. Borys, C. Ko, J. Suh, W. Fan, A. Thron, Y. Zhang, A. Buyanin, J. Zhang,
S. Cabrini, P. D. Ashby, A. Weber-Bargioni, S. Tongay, S. Aloni, D. F. Ogletree, J.
Wu, M. B. Salmeron, P. J. Schuck, *Nat. Commun.* **2015**, *6*, 7993.

[7]   V. Carozo, Y. Wang, K. Fujisawa, B. R. Carvalho, A. McCreary, S. Feng, Z. Lin, C.
Zhou, N. Perea-López, A. L. Elías, B. Kabius, V. H. Crespi, M. Terrones, *Sci. Adv.*
2017, *3*, e1602813.

[8]   a) S. Mouri, Y. Miyauchi, K. Matsuda, *Nano Lett.* **2013**, *13*, 5944; b) J. G. Kim, W. S.
Yun, S. Jo, J. Lee, C.-H. Cho, *Sci. Rep.* **2016**, *6*, 29813; c) F. Cadiz, E. Courtade, C.
Robert, G. Wang, Y. Shen, H. Cai, T. Taniguchi, K. Watanabe, H. Carrere, D. Lagarde,

M. Manca, T. Amand, P. Renucci, S. Tongay, X. Marie, B. Urbaszek, *Phys. Rev. X* **2017**, *7*, 21026.

[9] M. Amani, M. L. Chin, A. L. Mazzoni, R. A. Burke, S. Najmaei, P. M. Ajayan, J. Lou, M. Dubey, *Appl. Phys. Lett.* **2014**, *104*, 203506.

[10] S. Tongay, J. Suh, C. Ataca, W. Fan, A. Luce, J. S. Kang, J. Liu, C. Ko, R. Raghunathanan, J. Zhou, F. Ogletree, J. Li, J. C. Grossman, J. Wu, *Sci. Rep.* **2013**, *3*, 2657.

[11] a) L. Yang, X. Cui, J. Zhang, K. Wang, M. Shen, S. Zeng, S. A. Dayeh, L. Feng, B. Xiang, *Sci. Rep.* **2014**, *4*, 5649; b) Z. Lin, Y. Zhao, C. Zhou, R. Zhong, X. Wang, Y. H. Tsang, Y. Chai, *Sci. Rep.* **2015**, *5*, 18596.

[12] C. Neumann, S. Reichardt, P. Venezuela, M. Drögeler, L. Banszerus, M. Schmitz, K. Watanabe, T. Taniguchi, F. Mauri, B. Beschoten, S. V Rotkin, C. Stampfer, *Nat. Commun.* **2015**, *6*, 8429.

[13] a) M. Rahaman, R. D. Rodriguez, G. Plechinger, S. Moras, C. Schüller, T. Korn, D. R. T. Zahn, *Nano Lett.* **2017**, *17*, 6027; b) A. G. Milekhin, M. Rahaman, E. E. Rodyakina, A. V Latyshev, V. M. Dzhagan, D. R. T. Zahn, *Nanoscale* **2018**, *10*, 2755.

[14] M. Velický, G. E. Donnelly, W. R. Hendren, S. McFarland, D. Scullion, W. J. I. DeBenedetti, G. C. Correa, Y. Han, A. J. Wain, M. A. Hines, D. A. Muller, K. S. Novoselov, H. D. Abruña, R. M. Bowman, E. J. G. Santos, F. Huang, *ACS Nano* **2018**, *12*, 10463.

[15] Y.-H. Lee, X.-Q. Zhang, W. Zhang, M.-T. Chang, C.-T. Lin, K.-D. Chang, Y.-C. Yu, J. T.-W. Wang, C.-S. Chang, L.-J. Li, T.-W. Lin, *Adv. Mater.* **2012**, *24*, 2320.

[16] a) S. Berweger, M. B. Raschke, *Anal. Bioanal. Chem.* **2010**, *396*, 115; b) J. Stadler, T. Schmid, R. Zenobi, *Nano Lett.* **2010**, *10*, 4514; c) T. Deckert-Gaudig, A. Taguchi, S. Kawata, V. Deckert, *Chem. Soc. Rev.* **2017**, *46*, 4077.

[17] A. Chernikov, A. M. van der Zande, H. M. Hill, A. F. Rigosi, A. Velauthapillai, J.

Hone, T. F. Heinz, *Phys. Rev. Lett.* **2015**, *115*, 126802.

[18]   S. Tongay, J. Zhou, C. Ataca, J. Liu, J. S. Kang, T. S. Matthews, L. You, J. Li, J. C. Grossman, J. Wu, *Nano Lett.* **2013**, *13*, 2831.

[19]   S. Y. Yang, G. W. Shim, S.-B. Seo, S.-Y. Choi, *Nano Res.* **2017**, *10*, 255.

[20]   Y. Xie, Z. Wang, Y. Zhan, P. Zhang, R. Wu, T. Jiang, S. Wu, H. Wang, Y. Zhao, T. Nan, X. Ma, *Nanotechnology* **2017**, *28*, 84001.

[21]   M. López-Suárez, I. Neri, R. Rurali, *J. Appl. Phys.* **2016**, *119*, 165105.

[22]   A. Castellanos-Gomez, R. Roldán, E. Cappelluti, M. Buscema, F. Guinea, H. S. J. van der Zant, G. A. Steele, *Nano Lett.* **2013**, *13*, 5361.

Tip-Enhanced Photoluminescence in the gap-less mode, i.e. without the use of plasmonically active substrate, is utilized to discern local (tens of nm) inhomogeneities in the optoelectronic properties of as-grown MoS_2 monolayers. The results are put in contrast to measurements on exfoliated MoS_2. Special consideration is given to the edges, where photoluminescence enhancement and shift are observed in the grown MoS_2.

Tip-Enhanced Spectroscopy

A. Rodriguez, T. Verhagen, M. Kalbac, J. Vejpravova, O. Frank*

Imaging Nanoscale Inhomogeneities in As-Grown MoS2 by Tip-Enhanced Photoluminescence in Gap-Less Mode

ToC figure ((Please choose one size: 55 mm broad $\times$ 50 mm high **or** 110 mm broad $\times$ 20 mm high. Please do not use any other dimensions))